PAPER

Development of a large-area chip network with multidevice integration using a stretchable electroplated copper spring

IOP Publishing Journal of Micromechanics and Microengineering
J. Micromech. Microeng. **26** (2016) 025003 (15pp) doi:10.1088/0960-1317/26/2/025003

Development of a large-area chip network with multidevice integration using a stretchable electroplated copper spring

Wei-Lun Sung[1], Chih-Chung Chen[2], Kevin Huang[2] and Weileun Fang[1,3]

[1] Power Mechanical Engineering, National Tsing Hua University, Hsinchu, Taiwan
[2] imec Taiwan Inc., Hsinchu, Taiwan
[3] Institute of NanoEngineering and MicroSystems, National Tsing Hua University, Hsinchu, Taiwan

E-mail: fang@pme.nthu.edu.tw

Received 6 August 2015, revised 29 October 2015
Accepted for publication 9 November 2015
Published 18 December 2015

Abstract

This study designed and implemented the multidevice integration of a flexible large-area chip network using a stretchable electroplated copper spring. The functional devices are directly implemented and integrated on the nodes of a 2D chip network distribution, and the nodes are mechanically and electrically connected to surrounding nodes by stretchable copper springs. The springs can stretch and expand the distance between functional devices by several orders of magnitude to construct a large-area chip network with interconnected devices. The advantages of this approach are that (1) the existing and mature process technologies and materials for semiconductors in large-area applications are used, (2) stretchable electroplated copper springs with larger failure strain and good conductivity act as both mechanical and electrical connections between nodes, (3) rigid nodes act as hubs for device implementation and integration with microfabrication processes, and (4) the chip network can be applied to 2D curved (spherical) surfaces for flexible electronics. In application, the proposed expandable chip network using stretchable springs with integration of various devices (such as proximity and temperature sensors and light-emitting diode (LED) chips) has been successfully implemented and tested. The results show the chip network with integrated sensors performs as expected on a 2D plane distribution as verified by measurements. Moreover, LED chips have been integrated as an example to show that the proposed design can be used for flexible electronics applications.

Keywords: large-area electronics, chip network, stretchable spring, electroplate, proximity sensor, temperature sensor

(Some figures may appear in colour only in the online journal)

1. Introduction

Large-area electronics have attracted attention and have been extensively investigated in the past few decades. To date, various applications have been reported, such as organic light-emitting diode (OLED) lighting [1], solar cells [2], microsensors [3, 4] and wireless devices [5–7]. Compared with standard integrated circuits, a much larger footprint is required for these applications. Therefore, the cost per unit area is an important factor when evaluating the applicability in large-area electronics [8]. Few approaches can achieve structures suitable for large-area electronics applications, such as the conventional pick-and-place assembly method [6, 7, 9] and novel techniques such as printed organic (or inorganic) technologies [1–5, 10]. Pick-and-place assembly is a mature approach used to distribute electronic components over a large area. This approach is straightforward and has been used for a long time. In general, the picked chips are fabricated by conventional wafer-based semiconductor processes. Thus, the device chips are reliable and high performance. However,

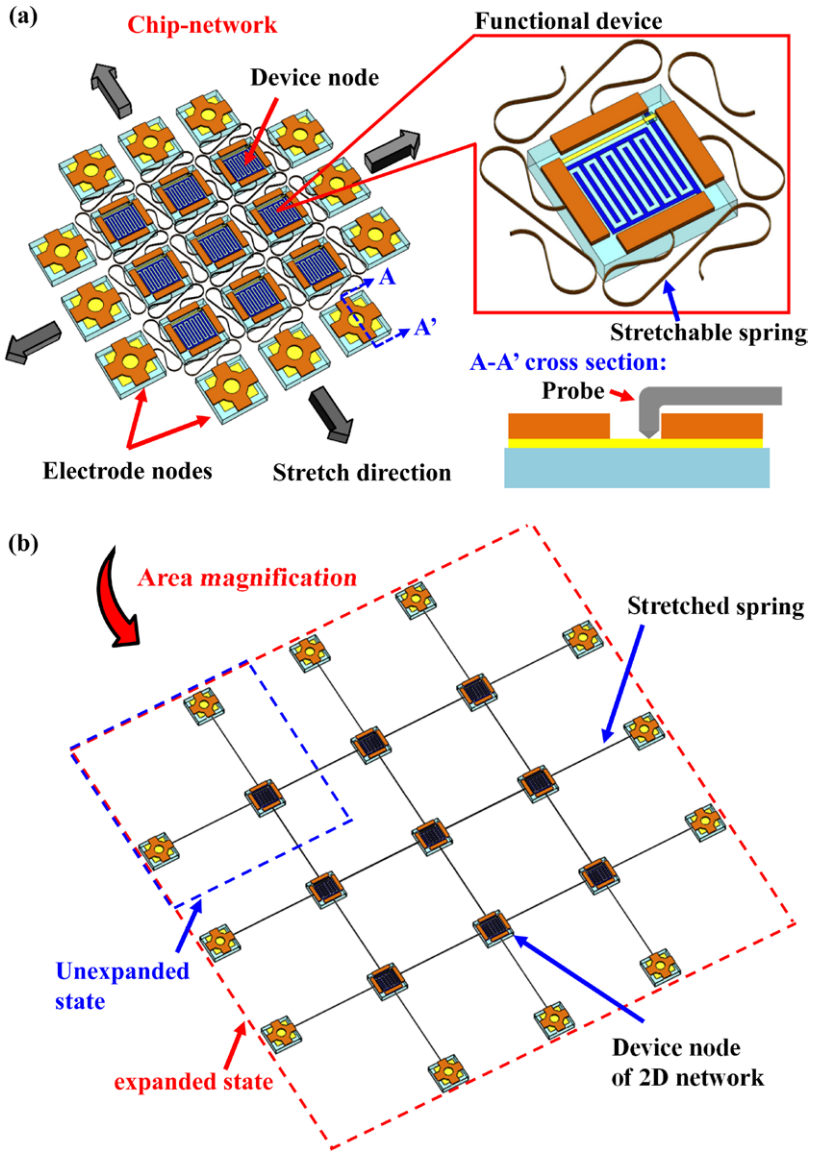

Figure 1. Schematic of a large-area 2D chip network with stretchable springs showing (a) the unexpanded chip network and (b) a magnified area after fully stretching the springs.

Table 1. Five types of spring designs for different stretching characteristics.

	Type 1	Type 2	Type 3	Type 4	Type 5
Spring shape				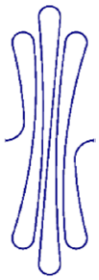	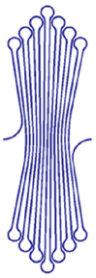
Initial length (distance between spring ends, mm)	0.7	0.7	0.7	0.7	0.7
Stretched length (mm)	5.35	5.05	8.18	12.17	27.92
Linear expansion factor	7.6	7.2	11.7	17.4	40
Max. strain (%)	3.8	2	4	6	8

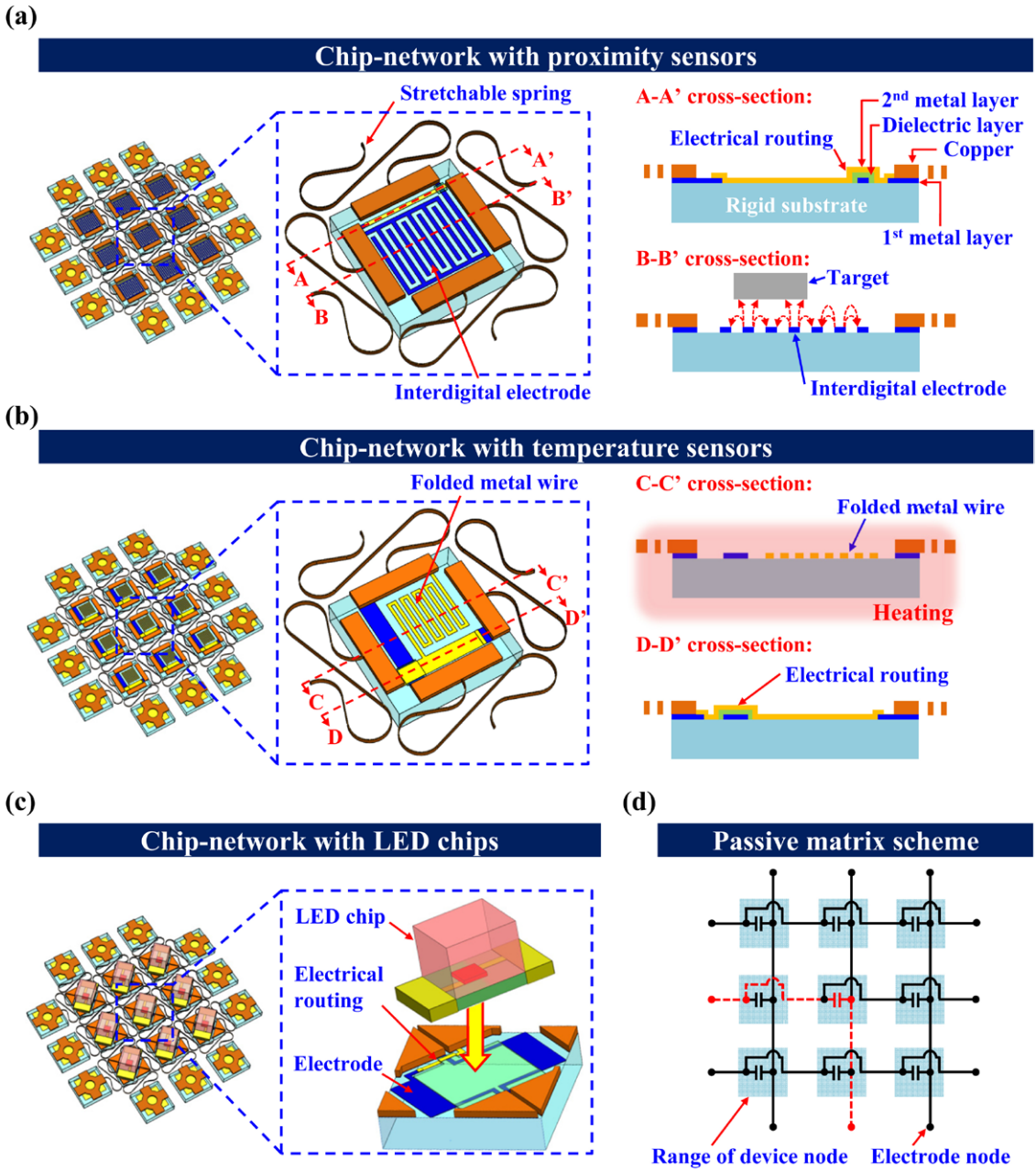

Figure 2. Schematic of a chip network integrated with functional devices by process integration with (a) proximity sensors and (b) temperature sensors and integrated by postassembly (c) LED chips, and (d) an electrical connection scheme of a chip network.

pick-and-place assembly is inefficient due to the fact that it is a serial process, and the cost per unit area is typically much higher than that of the other approaches. Moreover, it is difficult to accommodate curved surfaces during pick-and-place assembly. These drawbacks have limited the possibility of large-area applications using the pick-and-place method. Printed organic and inorganic technologies employ repetitive transferring or a printing method to define the pattern and structure. This approach is easier to apply to large areas and flexible substrates with much lower cost [8]. However, printed technologies are still lacking in device performance, reliability and the ability to integrate with electronics and microelectromechanical systems (MEMS) chips. Thus, the printed technologies have limited applications in large-area electronics due to an incompatibility with wafer-based semiconductor processes.

As a result, it is not straightforward to employ the above approaches to integrate the electronics and MEMS devices for large-area applications. To meet the requirements of various innovative larger-area electronics applications, one of the challenges is incorporating multifunctionality, flexibility, lower cost, and easier integration with conventional electronics and MEMS devices. One way to achieve these goals is to use stretchable springs to construct a chip network with interconnected functional devices and spread out the functional devices over a larger surface [11–20]. Thus, the coverage area of the chip network can be expanded, and the functional devices are discretized. For this approach, the

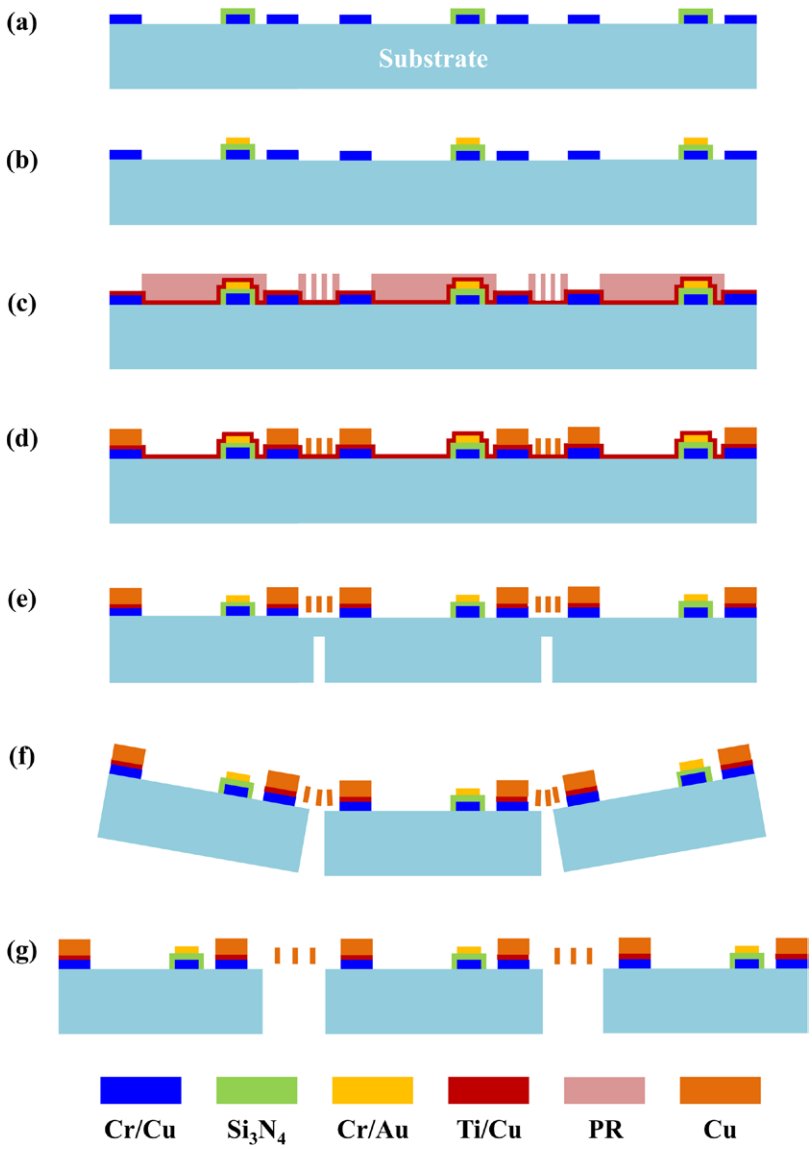

Figure 3. Fabrication process of a chip network with stretchable springs. (a and b) The first metal layer, Cr/Cu, dielectric layer Si_3N_4, and the second metal layer, Cr/Au, are deposited and patterned on the substrate. (c) Deposit of sacrificial and seed layer Ti/Cu and pattern photoresist (PR) mold (d) electroplate and removal of PR mode. (e) The backside splitting trench is defined by a dicing saw and the sacrificial and seed layer Ti/Cu is removed. (f) The backside splitting trench is broken. (g) The springs are stretched for large-area deployment.

functional devices can be fabricated close together in high density by modern microfabrication processes and spread out to cover a larger area at the time of deployment. As a result, the electronics and MEMS devices in the chip network have a higher performance, mature fabrication processes and compatibility with semiconductor and MEMS technologies. In addition, some studies have the stretchable springs attached to a flexible polymer substrate, and this can provide the function of flexibility to prevent devices and springs from becoming damaged during external loading [21, 22]. Chip networks with an expandable coverage area have been explored for various applications, such as an optical system with a curved image surface [11–13], structural health monitoring [14, 15] and a temperature sensor network [16]. The stretchable spring is implemented using silicon [11, 12, 14, 17] or polymer [13, 15, 16, 18, 19]. Clearly, the spring is a crucial component of a larger coverage area, since it needs to provide mechanical connection during the chip network expansion process as well as electrical conductivity to transmit signals or power between devices. Moreover, the nodes of the chip network act as hubs for device implementation and integration; therefore, they must be made of a rigid material in order to be compatible with conventional microfabrication processes.

Thus, this study extends the concept in [20] to design and implement a chip network integrated with functional devices. Electroplated copper is chosen to act as the stretchable spring because of its mechanical and electrical properties. Moreover, the functional devices can be implemented and integrated on rigid silicon (or glass) nodes using microfabrication processes. This study demonstrates that a chip network integrated with multifunctional devices (such as proximity and temperature sensors and LED chips) using stretchable electroplated copper

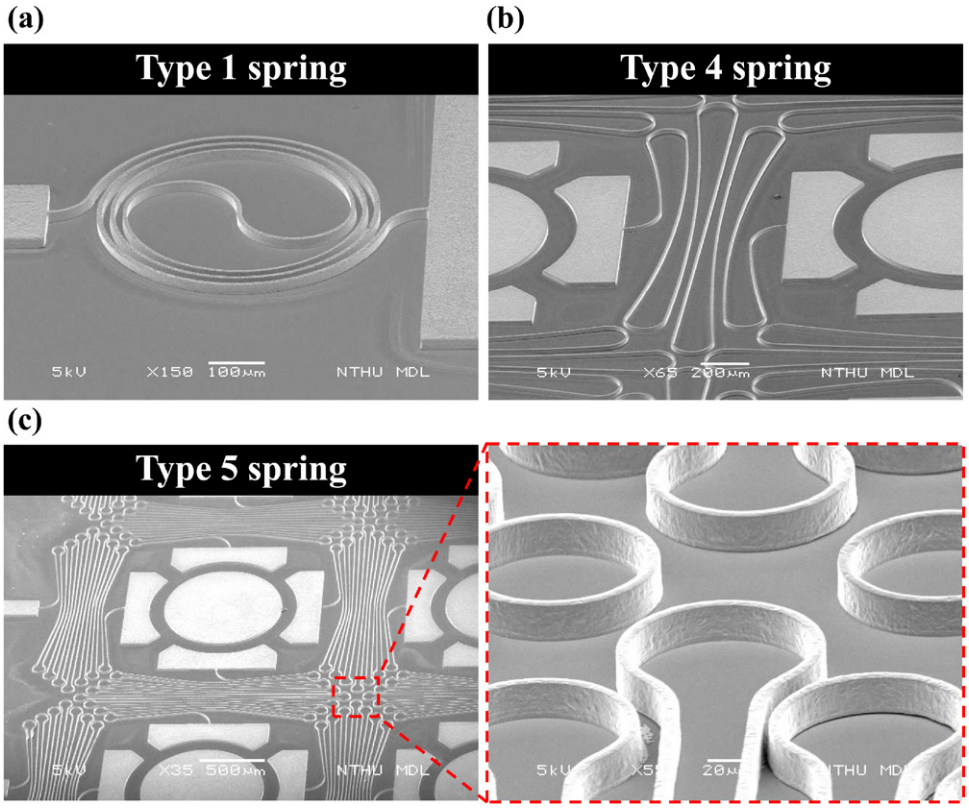

Figure 4. SEM micrographs of various spring designs. (a) Type 1 (spiral) spring. (b and c) Type 4 (b) and 5 (c) (serpentine) springs.

springs can be used for various flexible large-area electronics applications.

2. Concept and design

This study shows a different expanded area of the chip network by using different designs of stretched copper springs. The functional devices are directly implemented and integrated on the rigid silicon (or glass) nodes of the chip network. We will discuss the design concept of the chip network and integration schemes of these devices.

2.1. Schematic of an expandable chip network

The proposed design of the large-area 2D chip network architecture is shown in figure 1. Figure 1(a) shows an unexpanded chip network consisting of 3 × 3 device nodes, 12 electrode nodes and stretchable springs. The functional devices are fabricated on the device nodes, and the stretchable spring connects the surrounding device and electrode nodes. Moreover, the electrode nodes act not only as an inlet/outlet port for electrical signal/power transmission but also as the handling interface (as the probe mount shown in A–A′ cross-section) to stretch the chip network. The chip network can be expanded along a stretch direction from an unexpanded state to an expanded state, as indicated in figure 1(b). The flexible spring is stretched from a curved state to a straight line at full extension. Thus, the functional nodes of the 2D chip network are discretely and uniformity distributed over the area. By modifying the stretch length of spring, the distribution area of the chip network can be adjusted between the as-fabricated state to the full-expanded state.

Depending on the design of the spring, the coverage area of an expanded chip network can increase from several times to several orders of magnitude. This study designed five springs with different expansion factors, as shown in table 1. Type 1 is a spiral spring, and types 2–5 are serpentine springs with a different number of windings. The thickness and width of the springs are 20 μm and 10 μm, respectively. Moreover, as the stretchable springs are stretched to full extension (straight line), the maximum strain, $\varepsilon_{\max}$, encountered in the maximum curvature section is given by [14]

$$\varepsilon_{\max} = t/D$$

where t is the width of the spring defined by lithography process and D is the diameter of the maximum curvature of spring. For large-area electronics applications, this study uses electroplated copper as stretchable springs, which has the properties of being nonbrittle, and compatible with foundry fabrication processes. Copper springs also provide good mechanical properties for larger stretched length due to copper's higher failure strain (60% [23]) compared with silicon (1.7%) and good electrical properties for electrical paths between nodes. Considering the stretched length and process limit for the minimum line width, this study designs the maximum strain from 2%–8% for these five spring designs to form different expansion ratios of the chip network. The initial length

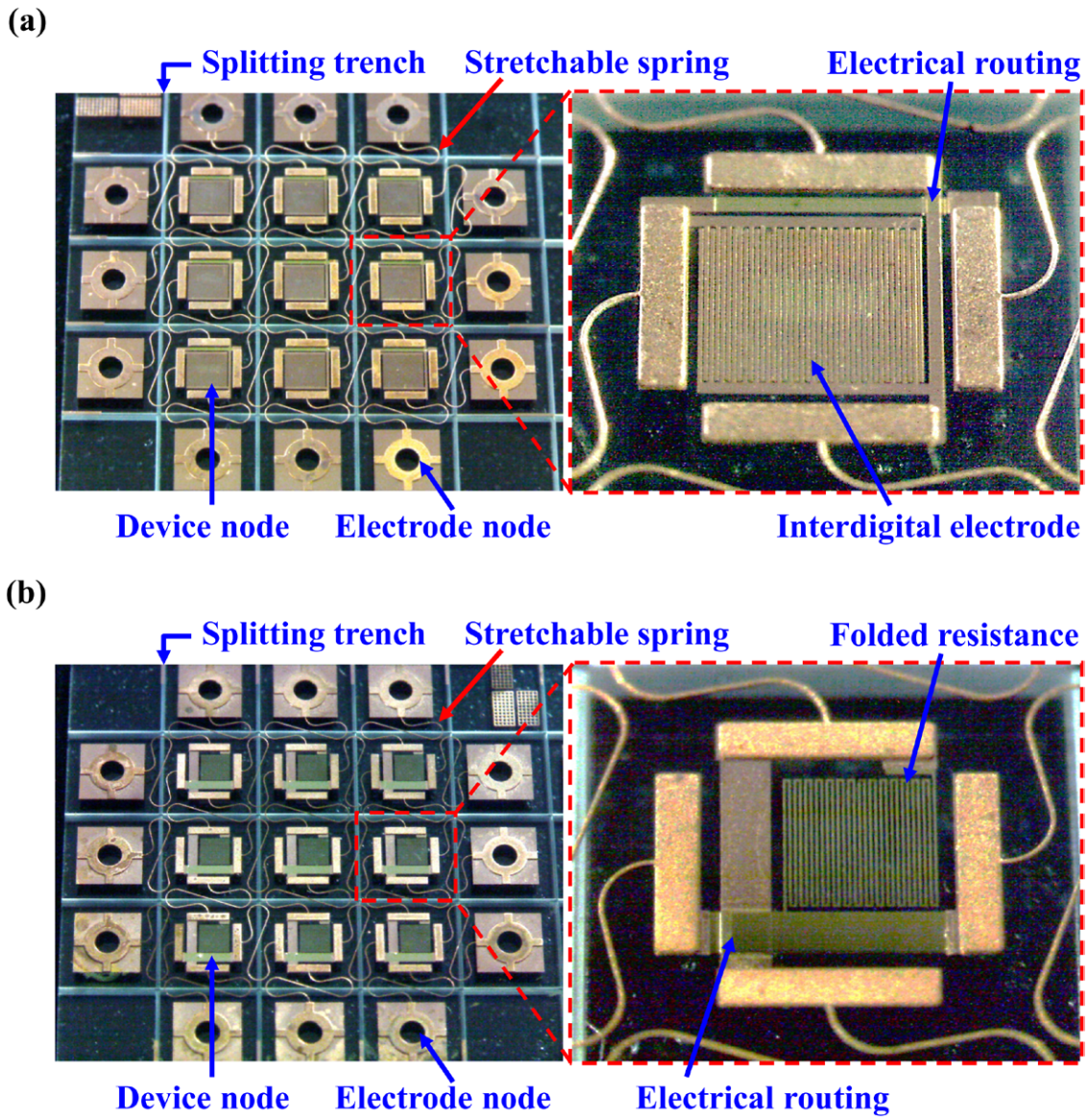

Figure 5. Typical fabrication results of an integrated sensor array, (a) proximity sensor array, and (b) temperature sensor array.

(distance between spring ends) of five springs is 0.7 mm, and the stretched lengths vary from 5.1 mm to 27.9 mm; thus, the linear expansion factor of these five types of springs varies from 7.2 times to 40 times, respectively.

2.2. Schematic of functional device integration

The proposed designs of the expandable chip network integrated with different functional devices are shown in figure 2. In this architecture, each functional device is fabricated or mounted on a rigid silicon (or glass) substrate before the 2D chip network is expanded. Thus, various electronic and MEMS devices can be easily implemented and integrated using a planar microfabrication processes. A chip network integrated with proximity and temperature sensors through process integration is shown in figures 2(a) and (b), and a network integrated with LED chips through postassembly is shown in figure 2(c). As indicated in figure 2(a), the chip network with proximity sensors is integrated through process integration. The proximity sensor is fabricated using standard wafer-based processing steps on the rigid nodes and is connects to surrounding nodes via stretchable springs. The electrical routing is formed by two metal layers and one dielectric layer to individually address each node of the chip network, as illustrated in A–A′ cross-section. In B–B′ cross-section, the 1st metal layer (Cr/Cu) acts as an interdigital electrode for the proximity sensor used to detect the distance between the sensor and the target (moving object). The sensing capacitance of the fringe electric field generated by the interdigital electrode varies as the distance between the target and the stationary interdigital electrode changes [24, 25]. The size of one single electrode is 860 μm (L) $\times$ 20 μm (W), and the gap between electrodes is 5 μm with a total of 20 pairs. Moreover, the area of each node is 2.3 mm $\times$ 2.3 mm. Using the same architecture in figure 2(a), a chip network with temperature sensors is shown in figure 2(b). The temperature sensor consists of electrical routing and folded metal wire for detecting ambient temperature [26–28]. The sensor measures resistance by the

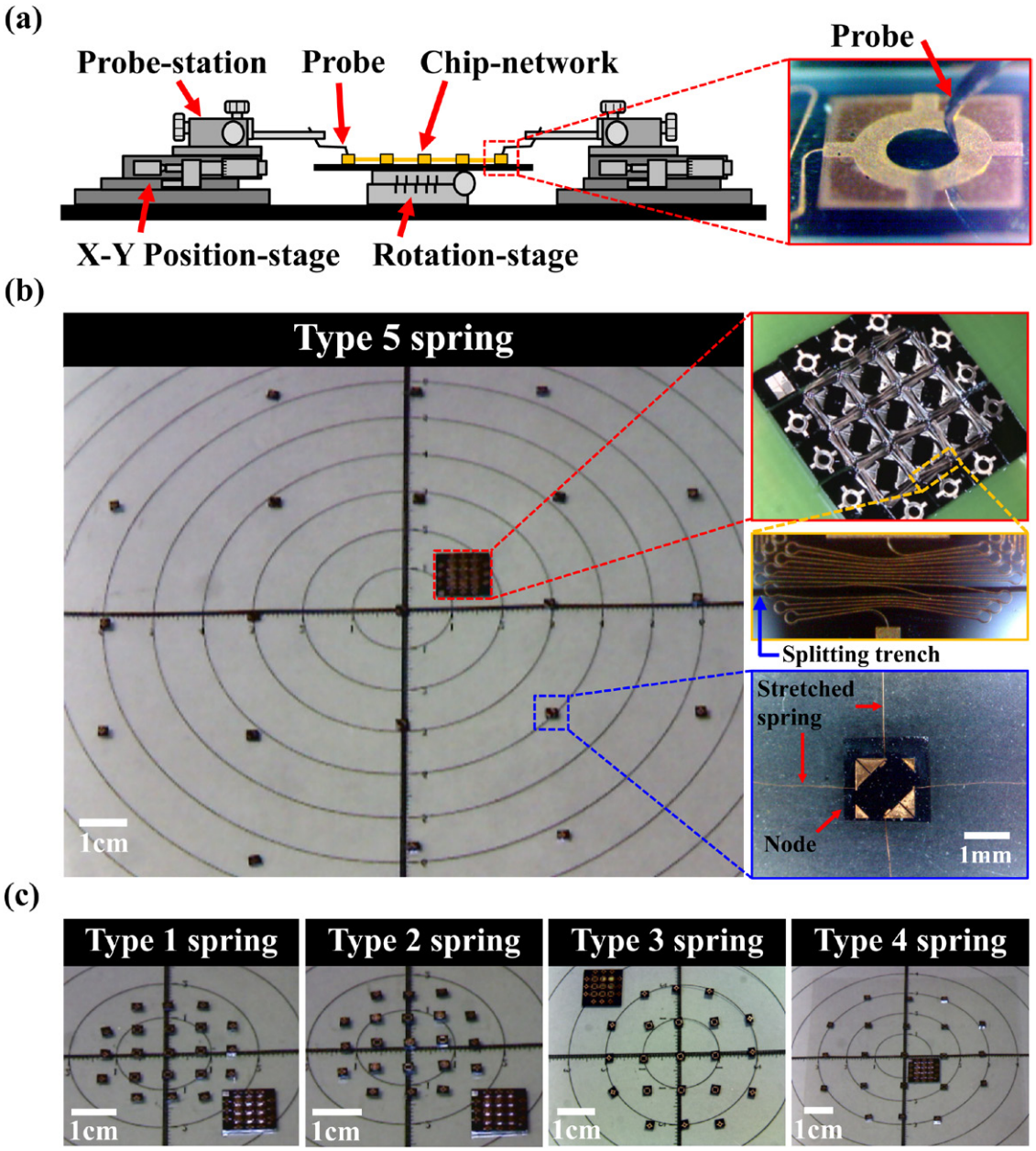

Figure 6. Stretching tests and results for mechanical connection. (a) Setup of the stretching tests. (b) Chip network with type 5 springs before and after stretching. (c) Results of stretching different types of springs.

folded metal wire, and the resistance will change as the ambient temperature varies, as shown in C–C′ cross-section. The 2nd metal layer (Cr/Au) acts as a metal wire, and it is chosen because it has a higher and more stable temperature coefficient of resistance (TCR) [27, 28]. The cross-section of folded metal wire is 10 μm (W) × 0.4 μm (H), and its total length is 21 mm. In D–D′ cross-section, the metal and dielectric layers for electrical routing of temperature sensors are also illustrated. Figure 2(c) shows a chip network integrated with LED chips using a postassembly method [29]. The metal and dielectric layers form the electrical routing and electrode on the node for electrical connection of the LED chips. The LED chips are then mounted on the nodes of the chip network. The commercially available LED chip is packaged, and the size is 1.6 mm (L) × 0.8 mm (W) × 0.8 mm (H). This study uses an LED chip as an example for testing and verifying the compatibility with semiconductor devices, and the LED chip can be replaced with a variety of electronic components. It is also noted that the process integration and postassembly methods can be modified by a variety of fabrication processes and wafer-level bonding of semiconductor/MEMS technology for various larger-area applications. Moreover, the electrical signal and power of each node can be individually addressed using a passive matrix scheme [30] as shown in figure 2(d). The middle capacitance element of the chip network can be measured by applying the corresponding electrode nodes (dotted line) while the other electrode nodes are shorted. The capacitance element can also be replaced by other electronic components such as resistance or inductance elements.

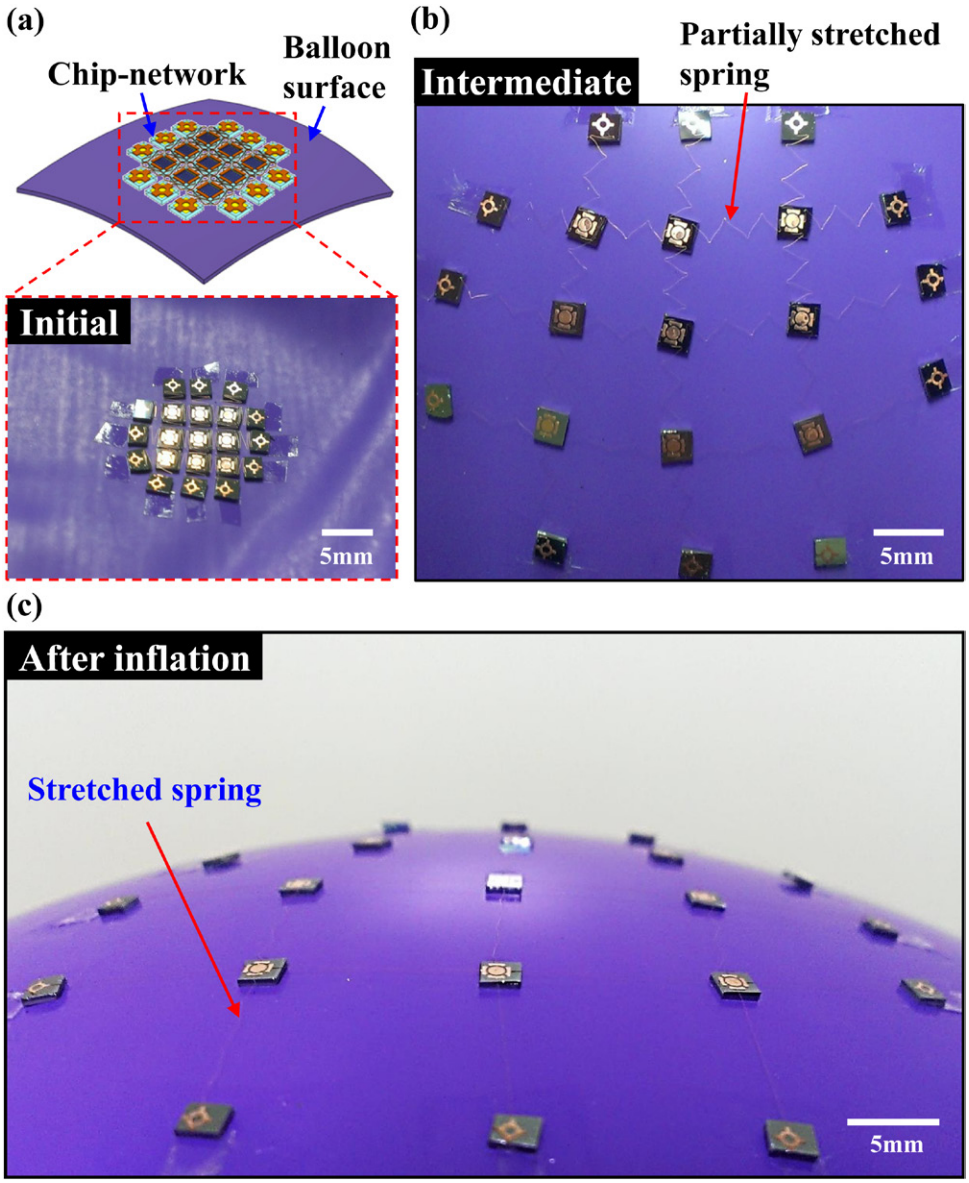

Figure 7. Demonstration of the capability of the 2D chip network on a curved surface by inflating a balloon. (a) Initially fixed on a deflated balloon. (b) Intermediate step. (c) The spring is stretched to its full length.

3. Fabrication process and results

The study exploits the existing process steps and materials to implement the expandable chip network and further integrate it with electroplated copper springs. Figure 3 shows the fabrication process steps of the presented approach. As shown in figure 3(a), the 1st adhesion and metal layers Cr/Cu (20 nm/200 nm) were deposited and patterned on the substrate. The metal layers acted as electrical routing and sensing electrodes of proximity sensors. After that, a 250-nm-thick Si_3N_4 film was deposited and patterned to act as a dielectric layer between the 1st and 2nd metal films and prevent oxidation of the 1st metal film. As illustrated in figure 3(b), the 2nd adhesion and metal layers Cr/Au (20 nm/400 nm) were deposited and patterned as the electrical routing and thermal resistance material of the temperature sensors. Figures 3(c)–(f) show the thick electroplated copper structure (20 μm) defined by photoresist molding. After that, the splitting trenches (by dicing saw) were used to separate each node. Detailed process steps are explained in [20]. Finally, as shown in figure 3(g), the chip network was ready to be stretched for large-area deployment. Note that the components on nodes can be fabricated using other approaches (such as bonding technology and bulk micromachining) to implement a variety of microdevices.

Figure 4 shows the fabrication results of various spring designs. Figures 4(a) and (b) show the scanning electron microscopy (SEM) micrographs of type 1 (spiral) and type 4 (serpentine) springs. The electroplated copper springs are suspended on the silicon substrate. The thickness and width of the copper springs are 20 μm and 10 μm, respectively. Figure 4(c) shows the SEM micrographs of the type 5 spring, and the zoom-in micrograph shows the location where the maximum stress occurred when the spring was stretched to full extension. The copper springs are fully suspended on the

substrate with a small air gap. Fabrication results of the integrated sensor array are shown in figure 5. Figure 5(a) shows the expandable chip network integrated with a proximity sensor array. The sensors are housed on the glass nodes and connected to the surrounding devices and electrode nodes by stretchable springs. Since the glass substrate is transparent, the backside splitting trench can be clearly observed. As indicated in the zoom-in micrograph, the proximity sensor consists of the electrical routing and interdigital electrode for detecting the distance between the sensors and the target (as shown in figure 2(a)). Figure 5(b) shows the expandable chip network integrated with a temperature sensor array. As indicated in the zoom-in micrograph, the temperature sensor consists of the electrical routing and folded resistance for detecting ambient temperature.

4. Test and measurement results

We performed various tests to evaluate the performances of the presented chip network. For instance, the stretching properties of the chip network and the performance of the functional devices were evaluated. The following discussion aims to provide the results of the stretching tests and the measurement results of device integration.

4.1. Stretching tests

In this section, a different expanded area of the chip network is formed with different designs of stretchable springs, and the results show that the springs are still connected after stretching is done on both an in-plane flat surface and a curved surface. Results of the stretching tests for mechanical and electrical connections are also included.

4.1.1. Mechanical connection of stretching tests. The in-plane stretching test setup and results are shown in figure 6. Figure 6(a) shows the setup used for the stretching tests. The probe on the probe station is fixed to the mount on the electrode nodes of the chip network, and the springs of the chip network are then stretched using the *X*-*Y* position stages. In general, the maximum stretchable distance of each spring is in the order of millimeters. Thus, the displacement of stretched springs can be precisely controlled (resolution: 10 μm) and further to avoid the rupture or overstretching of springs. The micrographs in figures 6(b) and (c) display the in-plane stretching test results for different spring designs. Figure 6(b) shows the stretching of the chip network connected by a type 5 spring design indicated in table 1. The right top micrograph in figure 6(b) shows the 11 mm $\times$ 11 mm chip network before stretching. The device and electrode nodes on the chip network have been split (as indicated in figure 3(f)) to allow the chip network to be expanded using this setup. The right middle and bottom micrographs in figure 6(b) respectively show the type 5 spring before and after stretching. After stretching from a serpentine shape to a straight line, the spring can still connect to the surrounding nodes and the chip network reaches its maximum coverage area. Note that the maximum force before

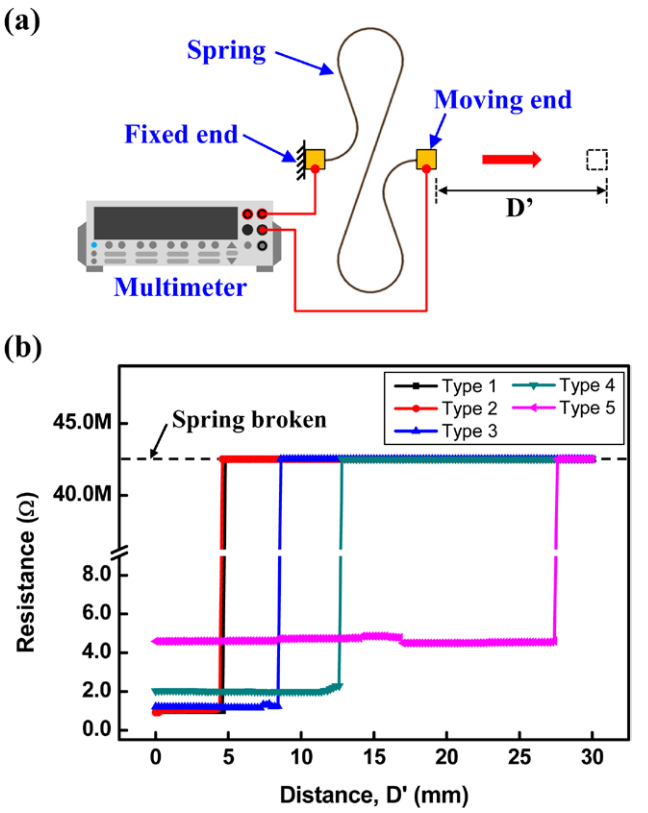

Figure 8. Stretching tests and results of electrical connection. (a) Setup of the stretching tests. (b) Measurement results of electrical connection for five types of springs.

rupture of the spring is measured by force gauge, and the force springs can withstand is 35.5 $\pm$ 2.12 mN. The left micrograph in figure 6(b) further displays the chip network after being fully stretched in a planar surface. The area of the chip network has increased from 11 mm $\times$ 11 mm (as shown in the right-top micrograph) to 121 mm $\times$ 121 mm. Thus, the chip network connected with a type 5 spring design has a maximum areal expansion of 121-fold after being fully stretched. Moreover, as indicated in figure 6(c), the areal expansion ratios of the chip network (same as the one shown in figure 6(b)) with type 1, type 2, type 3, and type 4 springs are 7.4-fold, 6.8-fold, 14.2-fold, and 27.5-fold, respectively. The test shows that the stretchable springs approach can provide large areal expansion from an initially small area (unexpanded state) to reduce the cost per unit area. Note that during the stretching process, each node is manually separated and controlled by the position stage. Thus, it is difficult to apply uniform loads on the chip network simultaneously, and the position offset of the chips is observed in figure 6.

Figure 7 demonstrates the capability of the 2D chip network stretched by a curved surface (the inflated balloon). Micrographs in figure 7(a) show an unexpanded 11 mm $\times$ 11 mm chip network connected with type 4 springs. The 12 electrode nodes of the chip network are initially fixed on a deflated balloon surface by tape. The 9 internal device nodes are floating and connected to surrounding nodes by stretchable springs. After that, the balloon is inflated to stretch the springs on a curved surface. The micrograph in figure 7(b)

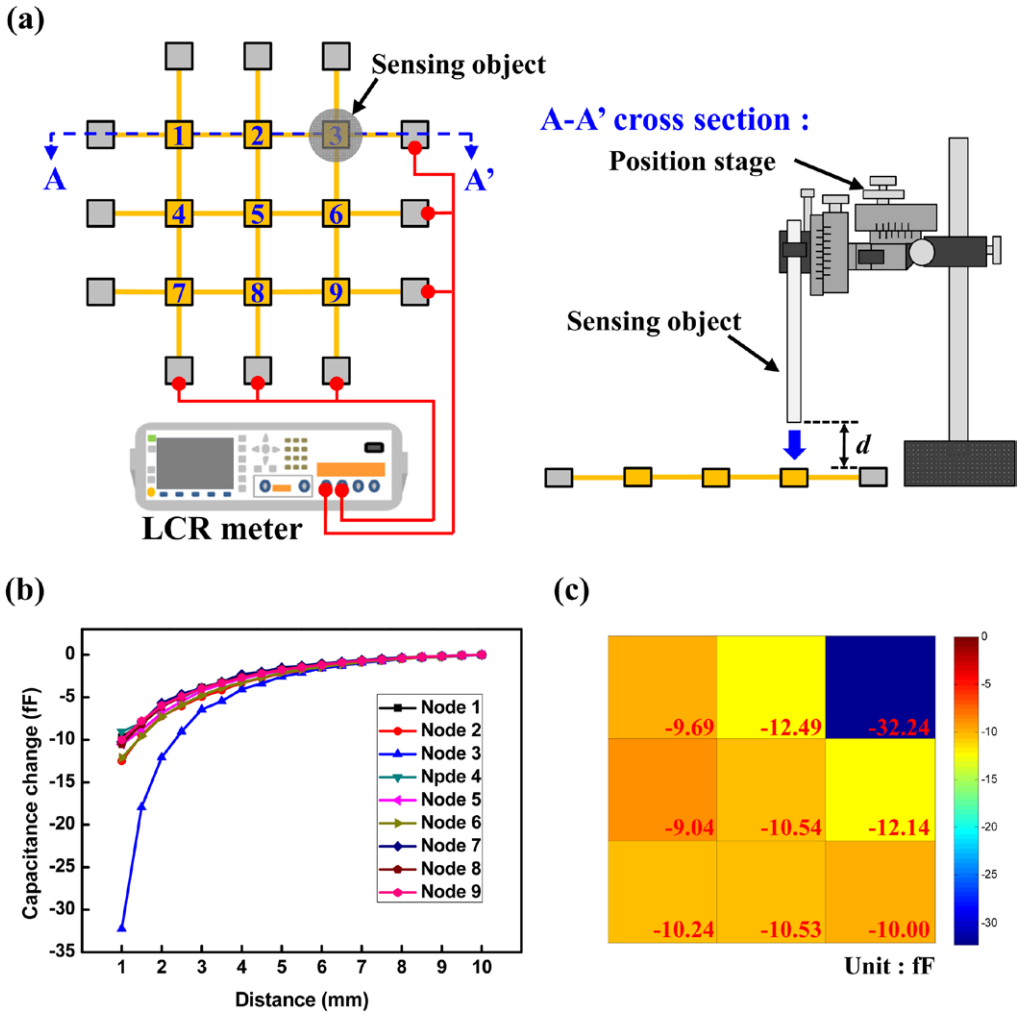

Figure 9. Proximity sensor of the chip network with a small sensing object. (a) Experimental setup. (b) Measurement results. (c) Pseudocolor plot of the results.

depicts type 4 springs that are partially stretched (but not yet fully stretched) by the inflated balloon. The area of the chip network is expanded to ~40 mm × 40 mm as the balloon is being inflated. Meanwhile, the device nodes of the chip network are distributed on a curved balloon surface. Finally, the springs are fully stretched on the inflated balloon as indicated in figure 7(c), and the area of the chip network is further increased to 56 mm × 56 mm. This test demonstrates that the flexible and stretchable springs allow the chip network to properly conform to a curved surface.

4.1.2. Electrical connection of the stretching tests. The stretchable copper spring serves not only as the mechanical connection but also as the electrical routings between the nodes. This study also performed electrical tests on the chip network. The resistance change of the springs while the spring is being stretched is shown in figure 8. Figure 8(a) shows the setup to characterize the resistance change of the spring during the stretching tests. The spring has one end fixed and the other end mounted on a position stage to specify its displacement. Thus, the stretching length of the spring is controlled with a resolution of 10 μm. The multimeter is used to measure the resistance change of the spring during the stretch tests. The measurements in figure 8(b) show the resistance change versus the stretching distance for the five types of springs. The results indicate that the type 1 design has an average resistance of 0.99 Ω and resistance variation of ±0.003 Ω during the extension of the spring. Moreover, the average resistances and variations for type 2–5 designs during the extension of the springs are 1.04 ± 0.049Ω, 1.19 ± 0.043 Ω, 2.02 ± 0.046 Ω and 4.62 ± 0.110 Ω respectively. As the stretched distances exceed the full extension, resistances increase drastically due to rupture of the springs. This test demonstrates the copper stretchable springs retain their electrical properties, and the variations of resistance change for type 1–5 springs are less than 4.7% during the stretching process. The slight resistance variation might influence the signal output from the device on the sensing node (e.g. the temperature sensor in figure 2(b)). Thus, calibration of the devices could be required after spring stretching.

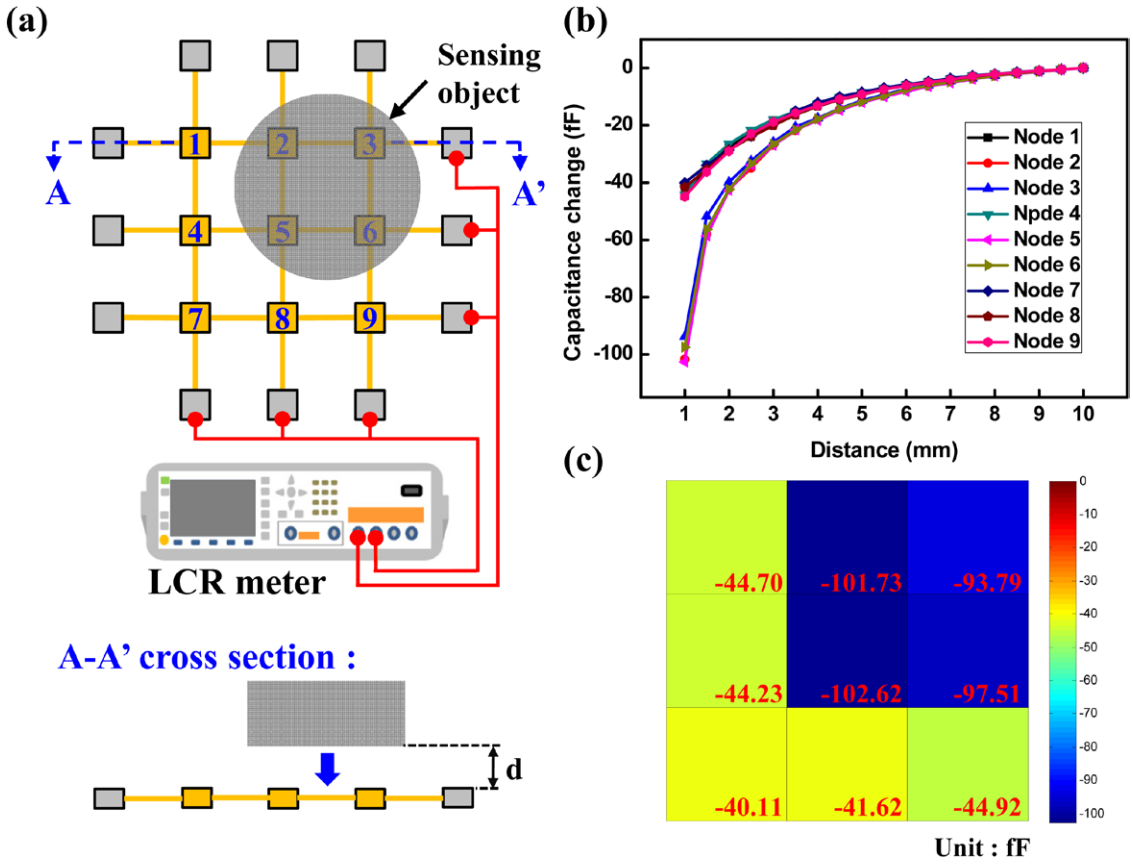

Figure 10. Proximity sensor array of the chip network with a large sensing object. (a) Experimental setup. (b) Measurement results. (c) Pseudocolor plot of the results.

4.2. Device integration

This study has successfully demonstrated the following three applications of chip network integration: (1) a proximity sensor chip network, (2) a temperature sensor chip network using process integration, and (3) an LED chip network using postassembly. The measurement results of these devices will now be discussed.

4.2.1. Integration I: proximity sensor chip network. Figure 9 shows the measurement results for the fabricated chip network shown in figure 5(a). The chip network consists of a 3 × 3 proximity sensors array connected by type 2 stretched springs. Figure 9(a) shows the experiment setup to characterize the performance of the proximity sensor network. In this test, the chip network has been stretched to 28 mm × 28 mm and then attached to a solid stage. The nine proximity sensors of different locations have been marked with the numbers 1–9. This study employed a metal (stainless steel) rod as the sensing object for the proximity tests. The diameter and length of the metal rod are 2 mm and 100 mm, respectively. As the object approaches the proximity sensors, the sensing capacitance is detected by the interdigital electrodes. The LCR meter (Agilent E4980A) is then used to measure the capacitance change, which is then recorded by a computer. The sensing object is moved vertically on top of sensor node 3 by position stage, and the distance, d, between the sensing object and the proximity sensor is shown in A–A′

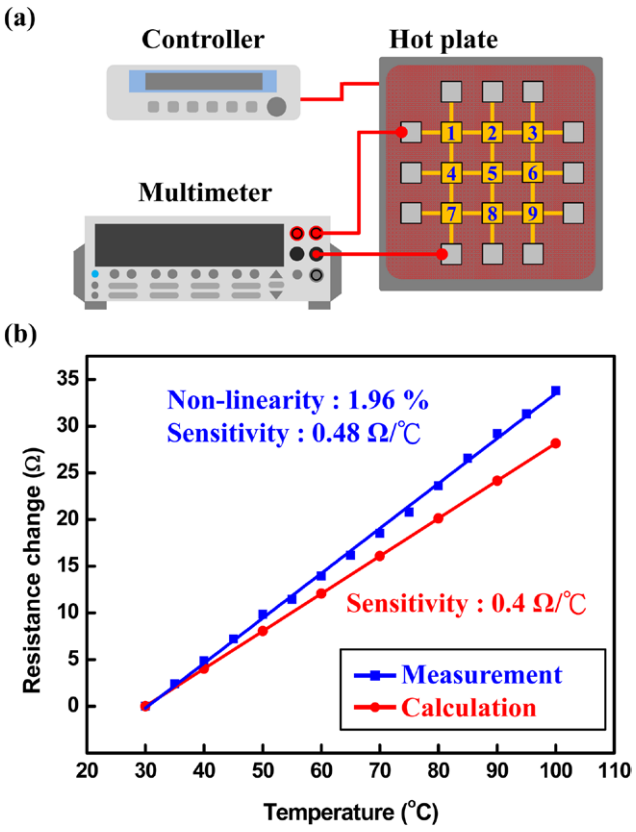

Figure 11. Temperature sensor of the chip network. (a) Experiment setup. (b) Comparison between experimental measurements and calculations.

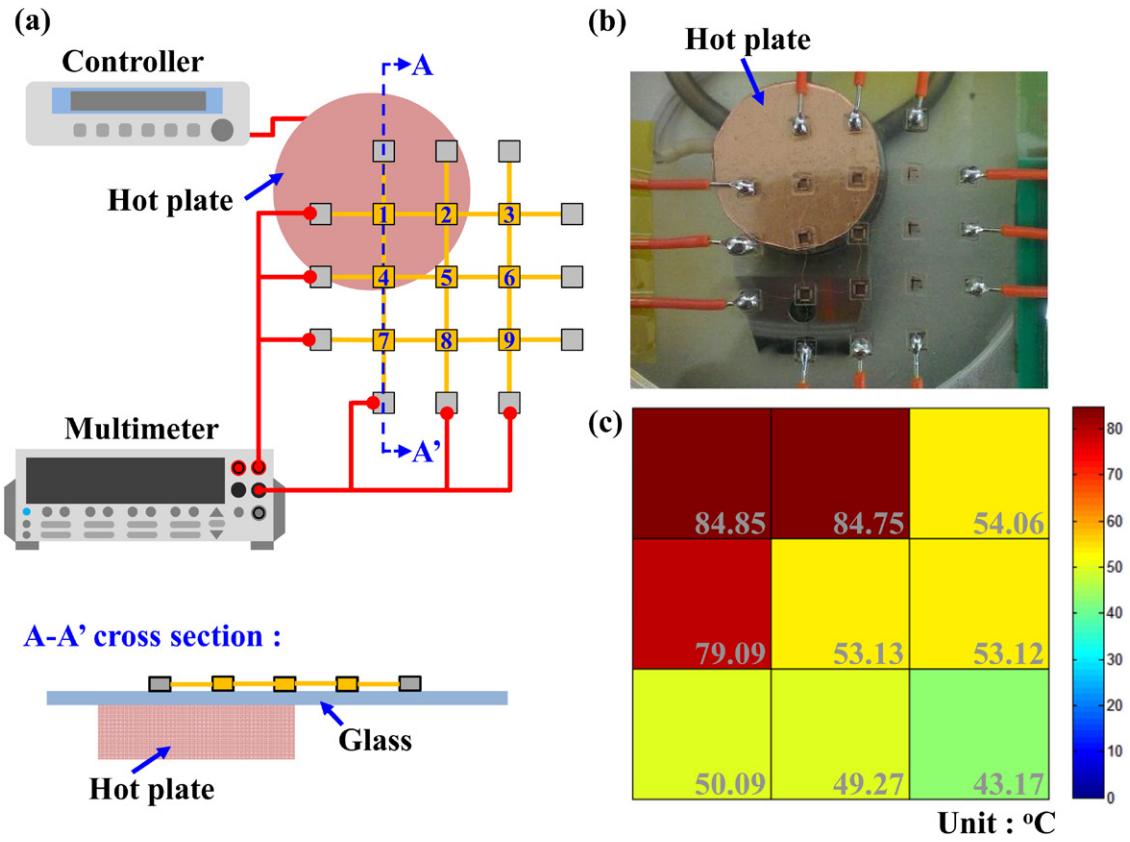

Figure 12. Temperature distribution of a larger object. (a and b) Experimental setup. (c) Pseudocolor plot of the measurement results.

cross-section. Moreover, the sensing object is mounted on the three-axis position stage to control the in-plane positions and height with a resolution of 10 μm. The typical measurement results recorded from the proximity sensors are shown in figure 9(b). The measurement results indicate that the total capacitance change recorded from node 3 is -32.24 fF as the sensing object moves from $d = 10$ mm to $d = 1$ mm. Note that the sensing capacitance changes from -6.46 fF to -32.24 fF as the sensing object moves from $d = 3$ mm to $d = 1$ mm. Hence, the capacitive proximity sensor of node 3 has a sensitivity of 12.09 fF mm^{-1} within a sensing distance of $d = 3$ mm to $d = 1$ mm. The measured initial capacitance of the proximity sensor (with no sensing object) is 4.4 pF. In addition, the capacitance changes of sensors other than node 3 are also measured and recorded in figure 9(b), as the sensing object moves on top of node 3. The capacitance change of node 3 is much larger than others within the range of proximity sensing distance (1 mm–3 mm). Figure 9(c) shows the pseudocolor plot of the capacitance change for each node as the sensing object moves to a distance of $d = 1$ mm on top of node 3. This plot clearly shows the location of the sensing object relative to that of the proximity sensors. The capacitance change is -32.24 fF on node 3, and the change on the other nodes is -9.04 fF to -12.49 fF.

By using the same experimental setup, the chip network with 3×3 proximity sensors is employed to detect a larger object. As shown in figure 10(a), the larger object (a steel rod 15 mm in diameter and 200 mm in length) will cover four sensor nodes such as 2, 3, 5, and 6. Figure 10(b) shows the measurement results in this test, which also indicate that the capacitance changes of the proximity sensors are significantly larger on nodes 2, 3, 5, and 6 than on the other nodes (nodes 1, 4, and 7–9). Figure 10(c) shows the pseudocolor plot of capacitance change as the large sensing object moves to a distance of $d = 1$ mm. The capacitance changes from -93.79 fF to -102.62 fF on nodes 2, 3, 5, and 6, while the other nodes see changes from -40.11 fF to -44.92 fF. This plot also clearly shows the location of the larger sensing object relative to the proximity sensors. Note that the coverage area of the chip network can be adjusted by the stretch length (partially or fully stretched) and the design of springs to meet the requirement of different applications and spatial resolution. Moreover, the chip spatial resolution is relative to the expansion area, and thus the limitations of the chip network can hardly simultaneously cover a large area with high resolution.

4.2.2. Integration II: temperature sensor chip network. Figure 11 shows the measurement results for the fabricated chip network shown in figure 5(b). The chip network consists of a 3×3 temperature sensors array connected by type 2 stretched springs. Figure 11(a) shows the measurement setup used to characterize the performance of the temperature sensors. Similarly, the chip network has been stretched to 28 mm $\times$ 28 mm, and the nine temperature sensors of different locations are also marked with the numbers 1–9. The chip network is

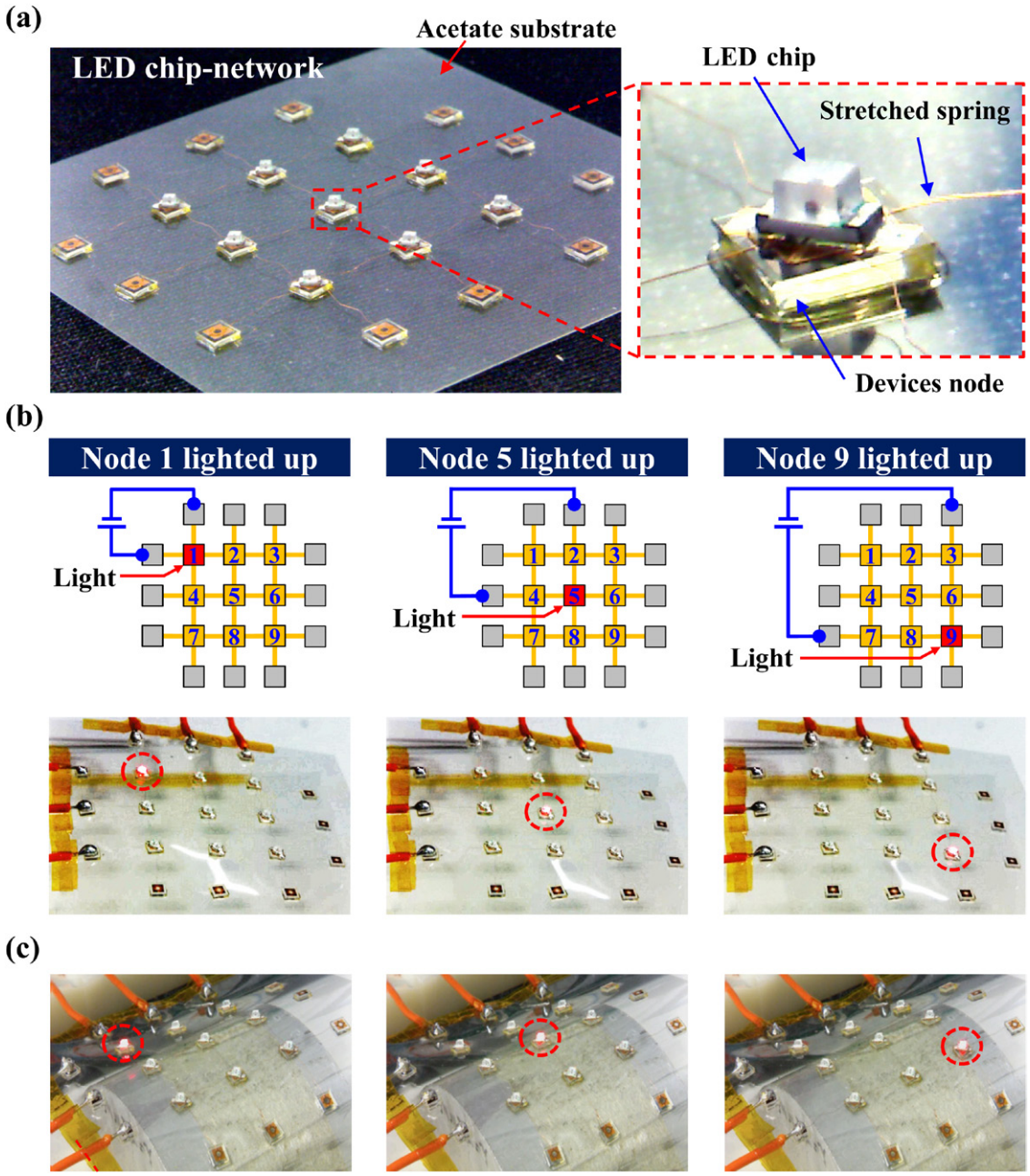

Figure 13. LED chips integrated with an expandable chip network. (a) LED chips are mounted on the device nodes and pasted on a flexible acetate substrate. (b) Lighting test for three LED nodes. (c) Lighting test on a curved surface.

attached to the surface of a commercial hot plate (Linkam Ltd., THMS600), which can control the temperature with a resolution of 0.1 °C. The resistance changes of temperature sensors are measured by the multimeter while the temperature is being adjusted. The measurement and calculation results of the temperature sensor are shown in figure 11(b). In comparison, the measured and predicted sensitivities are respectively 0.48 Ω/°C and 0.40 Ω/°C within the sensing range 30 °C–100 °C. Also, the measurement results indicate that the nonlinearity is 1.96% and the initial resistance is 202 Ω.

The characterization data in figure 11 of the chip network with 3 × 3 temperature sensors is further employed to detect the temperature distribution of a larger object. The chip networks in figures 11 and 12 are all stretched and also have the same stretched distance. Figure 12 depicts the temperature sensor chip network that is supported by a glass wafer (thickness is 500 μm), and a circular hot plate is attached to the left corner underneath the glass wafer. Thus, the hot plate is heating directly under nodes 1, 2, and 4, as shown in figures 12(a) and (b). Figure 12(c) shows the pseudocolor plot of the temperature distribution of the chip network with the hot plate controlled at a temperature of 90 °C. The temperature has been stabilized with a 10-min wait, and the resistance change is then measured for each of the sensors sequentially. By using the calibration curves in figure 11(b), the temperature distribution is determined by the chip network. The results indicate that nodes 1, 2, and 4 of the temperature sensor array observe temperatures ranging from 79.1 °C to 84.9 °C because they

are located directly on top of the hot plate (at 90 °C), and the other nodes (nodes 3 and 5–9) exhibit lower temperatures ranging from 43.2 °C to 54.1 °C caused by thermal conduction of glass wafer. As expected, node 9 records the lowest temperature since it is farthest from the hot plate.

4.2.3. Integration III: LED chip network. Finally, this study also shows the integration of LED chips with the presented chip network connected by type 2 springs, as shown in figure 13. The design scheme of this chip network is shown in figure 2(c). Unlike the cases of proximity and temperature sensors, which are integrated on the device nodes during fabrication, the LEDs are mounted on the device nodes using postassembly [29]. As illustrated in figure 2(c), the silver paste is coated on the electrodes of the device nodes using fluid dispensing systems for fixing and electrically connecting the LED chip to the electrodes on the device nodes. After mounting the LED chips, the chip network is heated to 230 °C for 60 min in order to cure the silver paste. The LED network is then expanded and pasted on a flexible acetate substrate, as shown in figure 13(a). Figure 13(b) shows the results of lighting tests on three different LED nodes. Nodes 1, 5, and 9 are lighted after applying 1.8 V into the corresponding electrode nodes. This indicates that the current is successfully transmitted through the stretched springs and electrical routing within the device nodes. The LEDs can be selectively controlled by applying voltages to different input and output electrode nodes. The lighting test further extends to cover a curved surface with a radius of curvature of 20 mm, as shown in figure 13(c). The results show that the stretched springs are still connected mechanically and electrically, and the LEDs light up successfully on curved surface. This test demonstrates the capability of the chip network for various flexible applications.

5. Conclusions

In summary, a large-area chip network integrated with functional devices using stretchable electroplated copper springs has been proposed and demonstrated. The copper springs, with larger failure strain and better conductivity as compared to silicon, act as both mechanical and electrical connections between nodes of the network. In addition, the nodes of the chip network easily act as hubs for device implementation and integration using microfabrication processes. Thus, this study has established the microfabrication processes to implement the presented chip network. The stretching properties of the chip network are implemented and evaluated. The chip network can achieve different areal expansion ratios by various designs of stretchable springs and retains the flexibility to cover curved surfaces. Moreover, the copper springs also provide sufficient electrical properties for many applications. During the stretching tests of the springs, the resistance change for different spring designs is less than 4.7%. Regarding the applications, this study has successfully demonstrated a chip network integrated with (1) proximity sensors, (2) temperature sensors (using process integration), and (3) LED chips (using postassembly). A chip network consisting of a 3×3 proximity sensor array is measured. The results show that the 3×3 sensor array provides the 2D location data for sensing objects of different sizes. Moreover, a chip network consisting of a 3×3 temperature sensor array is characterized. The measurements agree well with the predictions, and the 2D temperature distribution can be mapped by a 3×3 sensor array. Finally, the LED chips integrated with a chip network by postassembly are also demonstrated. The results show the LED chips light up normally in flat and curved surfaces. The present concept of a chip network with stretchable electroplated copper springs can be further integrated with various functional devices and microfabrication processes for large-area flexible electronics applications. In addition, the accuracy and reproducibility of the chip position offset can be improved as the chips are stretched by uniform loads in future experiments.

Acknowledgments

This research was sponsored in part by the Ministry of Science and Technology of Taiwan under grant number MOST 104-2221-E-007-016-MY3 and MOST 102-2221-E-007-027-MY3. The authors would like to thank imec Taiwan for technical and financial support. The authors also thank the Center for Nanotechnology, Materials Science, and Microsystems in National Tsing Hua University and Nano Facility Center of National Chiao Tung University for providing the fabrication facilities.

References

[1] Kopola P, Tuomikoski M, Suhonen R and Maaninen A 2009 Gravure printed organic light emitting diodes for lighting applications *Thin Solid Films* **517** 5757–62
[2] Krebs F C, Jorgensen M, Norrman K, Hagemann O, Alstrup J, Nielsen T D, Fyenbo J, Larsen K and Kristensen J 2009 A complete process for production of flexible large area polymer solar cells entirely using screen printing-first public demonstration *Sol. Energy Mater. Sol. Cells* **93** 422–41
[3] Chang W Y, Fang T H, Lin H J, Shen Y T and Lin Y C 2009 A large area flexible array sensors using screen printing technology *J. Disp. Technol.* **5** 178–83
[4] Molina-Lopez F, Quintero A V, Mattana G, Briand D and de Rooij N F 2013 Large-area compatible fabrication and encapsulation of inkjet-printed humidity sensors on flexible foils with integrated thermal compensation *J. Micromech. Microeng.* **23** 025012
[5] Sekitani T, Takamiya M, Noguchi Y, Nakano S, Kato Y, Sakurai T and Someya T 2007 A large-area wireless power-transmission sheet using printed organic transistors and plastic MEMS switches *Nat. Mater.* **6** 413–7
[6] Wu N C, Nystrom M A, Lin T R and Yu H C 2006 Challenges to global RFID adoption *Technovation* **26** 1317–23
[7] Want R 2004 Enabling ubiquitous sensing with RFID *Computer* **37** 84–6
[8] Arias A C, MacKenzie J D, McCulloch I, Rivnay J and Salleo A 2010 Materials and applications for large area electronics: solution-based approaches *Chem. Rev.* **110** 3–24

[9] Kahler J, Heuck N, Stranz A, Waag A and Peiner E 2012 Pick-and-place silver sintering die attach of small-area chips *IEEE Trans. CPMT* **2** 199–207
[10] Parashkov R, Becker E, Riedl T, Johannes H H and Kowalsky W 2005 Large area electronics using printing methods *Proc. IEEE* **93** 1321–9
[11] Rim S B, Catrysse P B, Dinyari R, Huang K and Peumans P 2008 The optical advantages of curved focal plane arrays *Opt. Express* **6** 4965–71
[12] Dinyari R, Rim S B, Huang K, Catrysse P B and Peumansa P 2008 Curving monolithic silicon for nonplanar focal plane array applications *Appl. Phys. Lett.* **92** 091114
[13] KO H C *et al* 2008 A hemispherical electronic eye camera based on compressible silicon optoelectronics *Nature* **454** 748–53
[14] Huang K and Peumans P 2006 Stretchable silicon sensor networks for structural health monitoring *Proc. SPIE* **6174** 617412
[15] Salowitz N, Guo Z, Li Y H, Kim K, Lanzara G and Chang F K 2012 Bio-inspired stretchable network-based intelligent composites *J. Compos. Mater.* **47** 97–105
[16] Guo Z, Kim K, Lanzara G, Salowitz N, Peumans P and Chang F K 2011 Micro-fabricated, expandable temperature sensor network for macro-scale deployment in composite structures *IEEE Aerospace Conf. (Big Sky, MT, 5–12 March 2011)*
[17] Huang K, Dinyari R, Lanzara G, Kim J Y, Feng J, Vancura C, Chang F K and Peumans P 2007 An approach to cost-effective, robust, large-area electronics using monolithic silicon *IEDM (Washington, DC, December 2007)* pp 217–20
[18] Lanzara G, Feng J and Chang F K 2010 Design of micro-scale highly expandable networks of polymer-based substrates for macro-scale applications *Smart Mater. Struct.* **19** 045013
[19] Zoumpoulidis T, Bartek M, Graaf P D and Dekker R 2009 High-aspect-ratio through-wafer parylene beams for stretchable silicon electronics *Sensors Actuators* A **156** 257–64
[20] Sung W L, Lai W C, Chen C C, Huang K and Fang W 2014 Micro devices integration with large-area 2D chip-network using stretchable electroplating copper spring *Proc. IEEE Int. Conf. MEMS (San Francisco, January 2014)* pp 1135–8
[21] Khang D Y, Jiang H, Huang Y and Rogers J A 2006 A stretchable form of single-crystal silicon for high-performance electronics on rubber substrates *Science* **311** 208–12
[22] Kim D H, Xiao J, Song J, Huang Y and Rogers J A 2010 Stretchable, curvilinear electronics based on inorganic materials *Adv. Mater.* **22** 2108–24
[23] Shah Q H 2006 Strain rate effect on the failure strain and hardness of metallic armor plates subjected to high velocity projectile impact *J. Eng. Sci. Technol.* **1** 166–75
[24] Wang D C, Chou J C, Wang S M, Lu P L and Liao L P 2003 Application of a fringe capacitive sensor to small-distance measurement *Japan. J. Appl. Phys.* **42** 5816–20
[25] Lo P H, Tseng S H, Yeh J H and Fang W 2013 Development of a proximity sensor with vertically monolithic integrated inductive and capacitive sensing units *J. Micromech. Microeng.* **23** 035013
[26] Resnik D, Vrtacnik D, Mozek M, Pecar B and Amon S 2011 Experimental study of heat-treated thin film Ti/Pt heater and temperature sensor properties on a Si microfluidic platform *J. Micromech. Microeng.* **21** 025025
[27] Yeh J H, Hong C, Hsu F M and Fang W 2011 Novel temperature sensor implemented on nanoporous anodic aluminum oxide template *IEEE Sensors (Limerick, October 2011)* pp 1253–6
[28] He S, Mench M M and Tadigadapa S 2006 Thin film temperature sensor for real-time measurement of electrolyte temperature in a polymer electrolyte fuel cell *Sensors Actuators* A **125** 170–7
[29] Chang C I, Tsai M H, Liu Y C, Sun C M and Fang W 2013 Pick-and-place process for sensitivity improvement of the capacitive type CMOS MEMS 2-axis tilt sensor *J. Micromech. Microeng.* **23** 095029
[30] Jang Y H, Lee K N and Kim Y K 2006 Characterization of a single-crystal silicon micromirror array for maskless UV lithography in biochip applications *J. Micromech. Microeng.* **16** 2360–8